High Recyclability Magnetic Iron Oxide-Supported Ruthenium Nanocatalyst for H2 Release from Ammonia-Borane Solvolysis

Didier Poinsot, Moad Bouzid, Agathe Burlot, Clève D Mboyi, Pierre-Emmanuel Doulain, Jérémy Paris, Olivier Heintz, Bruno Domenichini, V. Collière, Myrtil L Kahn, et al.

High Recyclability Magnetic Iron Oxide-Supported Ruthenium Nanocatalyst for H_2 Release from Ammonia-Borane Solvolysis

Didier Poinsot,[a] Moad Bouzid,[a,b] Agathe Burlot,[a] Clève D. Mboyi,[a] Pierre-Emmanuel Doulain,[c] Jérémy Paris,[c] Olivier Heintz,[b] Bruno Domenichini,[b] Vincent Collière,[d] Myrtil L. Kahn,[d] and Jean-Cyrille Hierso*[a]

[a] D. Poinsot, A. Burlot, M. Bouzid, Dr. C. D. Mboyi, Pr. Dr. J.-C. Hierso
Institut de Chimie Moléculaire de l'Université de Bourgogne (ICMUB – UMR CNRS 6302)
Université Bourgogne – Franche-Comté (UBFC), 21078 Dijon Cedex, France
Email: jean-cyrille.hierso@u-bourgogne.fr; orcid.org/0000-0002-2048-647X
[b] M. Bouzid, Dr. O. Heintz, Pr. Dr. B. Domenichini
Laboratoire Interdisciplinaire Carnot de Bourgogne (ICB − UMR CNRS 6303)
Université Bourgogne – Franche-Comté (UBFC), 21078 Dijon Cedex, France
[c] Dr. P.-E. Doulain, Dr. J. Paris
"Synthesis of Nanohybrids" SON – SAS
9, Avenue Alain Savary, 21000 Dijon France
[d] V. Collière, Dr. M. L. Kahn
LCC-CNRS, Université de Toulouse, INPT, UPS, 31077 Toulouse Cedex 4, France

Abstract: We report the high capacity of recycling of a technologically simple, easily recoverable, Ru@Fe_3O_4 magnetic nanocatalyst, efficient in the release of H_2 from ammonia-borane (AB) solvolysis, using H_2O or methanol at room temperature (25 °C). The initially oxidized Ru small nanoparticles (2-4 nm) are well-dispersed on an iron oxide support (*i. e.* super paramagnetic iron oxide of spinel structure, SPIO, as aggregates of 20 nm to a few μm). As nanocatalyst, this composite achieved short-time (<10 min) AB full hydrolysis (3 equiv H_2, no NH_3, [AB] = 0.1 mol L^{-1}) with a turnover frequency (TOF) of *ca* 20 min^{-1} (86 min^{-1} at 50°C). The post-catalysis characterization of the composite showed the formation of well-defined crystalline hcp Ru(0) dispersed on the SPIO. The activity for full H_2 release from AB is conserved over ten cycles, which is among the most effective recycling processes reported to date (a magnetic recycling is achieved in <2 min). Pleasingly, an even superior activity was found in the more challenging AB methanolysis, with a TOF up to *ca* 30 min^{-1} for full H_2 release, achieved in a recycling process repeated over 8 cycles.

Introduction

Recoverable benign heterogeneous catalysts are critical for addressing current environmental and economic challenging issues.[1,2,3] The role of nanomaterials is determining in this regard because of their unique physicochemical properties and large-scale applicability.[4,5,6] Accordingly, nanocatalysts often fill the gap between homogeneous and heterogeneous catalysts in terms of structure and activity.[7] However, from a general perspective nanocatalysts suffer from a major limitation, which is their efficient recovery.[8,9] Besides expensive advanced technologies, such as nanofiltration or ultracentrifugation,[10,11] conventional filtration techniques often result in the loss of materials, a limitation that impedes the application of nanocatalysts from economic and sustainability viewpoints. A low-cost pertinent approach is the formation of multifunctional nanocomposites, in which, in addition to the desired catalytic functionality, a magnetic property that can be activated under a magnetic field is introduced.[12] Insoluble magnetic nanocomposites thus provide a means of separation of the catalyst from the reaction mixture by employing a suitable external magnet. This approach obviates any centrifugation step, high-tech filtration devices, and other tedious workup processes. Magnetic supports, like iron-oxides, are now easily accessible for catalysis from many nanocomposite synthetic approaches,[5,8,9,12]. Thus, a lot more of reusable nanocatalysts can be tested and investigated in various topical reactions.

Herein, we investigated the catalytic properties of commercially available Ru@Fe_3O_4 and Ni@Fe_3O_4 for H_2 evolution from hydrolysis and methanolysis of ammonia-borane (AB) at room temperature (RT), Eq. 1. While a great deal of attention has been devoted to organic synthesis and cross-coupling reactions using transition metals supported on magnetically recoverable supports,[5,8,9,12] only a relatively limited attention has been devoted to similar recycling strategies for hydrogen storage and evolution from AB hydrolysis.[13] H_2 conventional physical storage under high pressure and/or low temperature under gas or liquid forms remains delicate from technological and economic requirement and societal acceptability. Chemical storage promoted by efficient catalysts using solid H_2 storage is thus regarded as the key solution to be developed. In this context, AB hydrolysis is of great interest.

$$H_3NBH_3\,(aq) + 2\,H_2O \longrightarrow NH_4^+\,(aq) + BO_2^-\,(aq) + 3\,H_2\,(g)$$

Early on, Xu and coworkers evidenced the interest of iron particle catalyzed hydrolytic dehydrogenation of AB,[14] although the activity was low, with a turnover frequency for H_2 evolution, (TOF) estimated at *ca* 3 $mol_{H2}min^{-1}mol^{-1}_{catal}$ (also denoted min^{-1}), the recyclability by magnetic decantation was proved. Following this work, the performances of magnetically recoverable nanocomposites based on expensive precious metals (Pd,[15,16,17] Pt,[18] Rh,[17,19,20]), or combining sophisticated multimetallic,[21,22,23,24,25,26,27] or multi-supports assembly has been illustrated.[28,29,30,31] A general feature of these systems, while they could be beneficial in terms of TOFs, is often their progressive strong deactivation after 3 to 5 recycling runs. This is also true for ruthenium-based systems. For illustration, Table

S1 (AB hydrolysis) and Table S2 (AB methanolysis), in the Supporting Information (SI), detail the data available for the performances and cycling stability of the recently reported ruthenium-based systems for H_2 evolution from AB solvolysis. A strict comparison is, however, not possible since in general the reactions conditions are clearly not unified with significant differences in work temperatures, concentrations, metal loading, systems characterization, TOF mode of calculation, *etc.* In addition, TOF is only a limited formal indicator, while the systems are not up-scaled as economically viable and ecologically sustainable industrial processes. Nevertheless, the examination of the Tables S1 and S2 clearly show that less than 10% of the reported systems reach up high recyclability (10 cycles or more), and that methanolysis is poorly investigated, to date.

Ruthenium is the most economically-competitive platinum group metal,[13] and concerning Ru-based magnetically recyclable systems, Öztürk and Özkar only very recently reported carbon-coated iron supports obtained by co-processing of Fe powders with methane in a radiofrequency thermal plasma reactor that were further impregnated either with Ru, Pd or Rh.[17] These systems achieved very good activity for AB hydrolysis (with TOFs *ca* 30-90 min^{-1}) that were fully conserved other five recycling runs. A full activity is not frequently conserved after such number of cycles. In the present work, we focused our attention on the recyclability of technologically simpler systems achieved by hydrothermal reaction of cheap transition metal salts in basic media,[32] *i. e.* Ru@Fe_3O_4 and Ni@Fe_3O_4 and commercially available. The recyclability experiments have demonstrated for 7%-Ru@Fe_3O_4 a number of cycles with a good activity conservation among the highest reported to date for AB hydrolysis and remarkable performances in methanolysis.

Results and Discussion

Ruthenium and nickel nanocomposites characterization. We first conducted elemental analysis and surface analysis of the nanocatalysts at various metal content elaborated from metal chlorides ($RuCl_3{\cdot}3H_2O$ and $NiCl_2{\cdot}3H_2O$) with preformed Fe_3O_4 magnetic nanoparticles (SPIO), using scanning electron microscopy (SEM), transmission electron microscopy (TEM) and X-ray photo electron spectroscopy (XPS). The samples prepared at a 7.0 wt. % target metal loading (Table 1, first and last entries) achieved this content as we found from energy-dispersive X-ray analysis (EDX, Figure S1 in Supporting Information, SI), X-Ray fluorescence, and inductively coupled plasma atomic emission spectroscopy (ICP-AES). Because of this economically-viable lower metal content, we focused on these nanocatalysts for further characterizations and related AB hydrolysis catalytic investigation and recycling performances.

TEM analysis showed for the supporting Fe_3O_4 iron oxide particles with a crystallite size above 20 nm, which form aggregates of higher dimension above 50 nm up to few μm (Figure S2 in SI). These nanoparticles exhibit superparamagnetic behavior at room temperature since their magnetization is cancelled out when the external magnetic field disappears. A typical TEM image of 7%-Ru@Fe_3O_4 nanocomposites is shown in Figure 1 (top, scale bar 20 nm) and revealed a good distribution

Table 1. Determination of weight metal content from Ni@Fe_3O_4 and Ru@Fe_3O_4

Metal	% target wt.	% EDX	% X-Ray fluo.	% ICP-AES
Ni	7.0	6.8 ± 0.1	6.8	6.5 ± 0.5
Ni	15.0	13.0 ± 0.6	14.7	12.6 ± 0.9
Ni	30.0	21.6 ± 0.5	25.1	19.7 ± 1.4
Ru	7.0	8.8 ± 0.2	7.8	7.4 ± 0.5

of much smaller crystallite of approximate size centered around 2-4 nm, which are identified as Ru-based nanoparticles (see also Figure S3 in SI). This was confirmed by the XPS of the Ru@Fe_3O_4 nanocomposite, shown in Figure 1 (full range survey XPS spectrum in Figure S4). Two components are observed from consistent decomposition of Ru 3d energy band. The Ru $3d_{5/2}$ band shows two components located at 281.1 eV and 281.8 eV, a higher formal oxidation degree than expected for fully reduced Ru(0). We confirmed the absence of Ru(0) by comparison with a reference made from pure zerovalent ruthenium, for which the binding energy of the Ru $3d_{5/2}$ was found at 280.2 eV (Figure S5). According to Pourbaix's diagram, the component at 281.1 might be attributed to Ru(IV), tentatively attributed to RuO_2 or ruthenium oxi-hydroxide [RuOx(OH)y] present on the surface, in relation with an OH^- rich synthetic medium. The second component at 281.8 eV is related to an even more oxidized phase that is probably less oxidized than RuO_3, which is known to exhibit a component around 282.4 eV.[33]

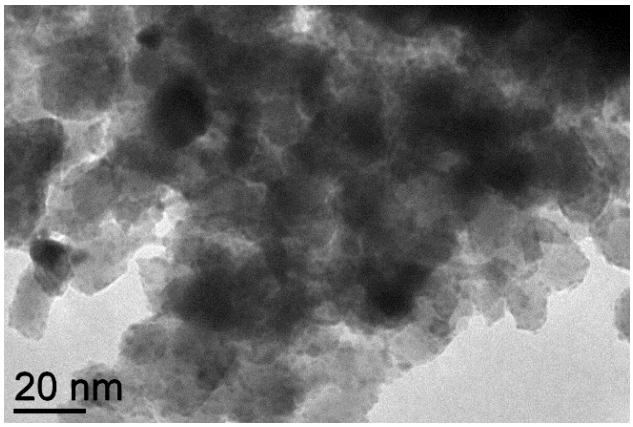

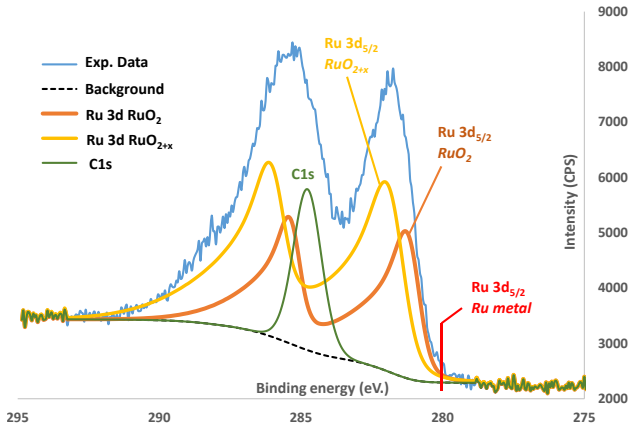

Figure 1. TEM image of 7%-Ru@Fe_3O_4 nanocomposite (top). High-resolution XPS spectra at the Ru 3d binding energy of 7%-Ru@Fe_3O_4 (bottom, calibration of the spectrum by the signal C 1s at 284.8 eV). The parameters used for decomposition analysis are given in SI (Figure S6).

Importantly, no potentially polluting chlorine is detected at the surface by XPS, clearly suggesting that $RuCl_3$ totally dissociates to release Ru^{3+} ions in the hydroxyl basic medium.

In the composite 7%-Ni@Fe_3O_4, while the presence and content of nickel was consistently established by EDX and ICP-AES, the corresponding TEM analysis did not allow to clearly observing Ni crystallite that would be distinct from iron oxide aggregates (Figure S7). This is presumably attributed to the proximate mass of Fe and Ni, which does not induce sufficient contrast in TEM, in contrast to the case of Ru@Fe_3O_4 nanocomposites (see Figures S8-S10 for complementary XRD and TEM structural data). XPS analyses carried out on 7%-Ni@Fe_3O_4 shows the Ni 2p that can be decomposed into a main band at 855.1 eV and a broad satellite at around 860.4 eV (Figure S11). These binding energy values indicate that $NiCl_3$ is mainly reduced to Ni(II), as possibly surface hydroxide, like typically $Ni(OH)_2$.[34,35]

Ammonia-borane hydrolysis from metal nanocomposites on iron oxide. Hydrolysis of AB was conducted at 25 °C (regulated water bath) using a stirred suspension of the nanocomposite in water, further injected with a freshly prepared aqueous solution of AB at 0.1 mol L^{-1} (3.0 wt. % of metal/AB) and monitored over time during up to 35 min. The volume of H_2 evolution was measured.

The nanocomposite 7%-Ru@Fe_3O_4 was found an effective catalyst in the first AB hydrolysis reaction we achieved, with a reaction completed (3 equiv H_2 produced) after 30 min, for a turnover frequency (TOF) about 10.0 mol H_2 min^{-1} mol^{-1}_{metal} (given here as min^{-1}). We observed an activation time of *c. a.* 8 min before the reaction begins with H_2 evolution.

We also tested the AB hydrolysis reaction in the presence of pristine SPIOs only, under otherwise the same conditions, without observing any H_2 evolution, even after 72 h stirring at RT. This confirmed that the iron oxide magnetic support itself does not promote any AB hydrolysis.

After a first catalytic run, the nanocomposite was magnetically quickly recovered by using a simple magnet block settling and syringing out the supernatant (Figure 2). Without any further treatment, a subsequent run (2^{nd} cycling) was achieved with the introduction of a 0.1 mol L^{-1} fresh AB aqueous solution. We observed the disappearance of the induction time that occurred in cycle 1, with an immediate H_2 evolution yielding again three equiv. of H_2 in about 12 min, and corresponding to an average TOF *ca* 18.0 ± 0.5 min^{-1}. The monitoring of the cycles 3 to 7 evidenced a conservation of this activity for the ruthenium nanocatalyst, and only cycles 8 to 10 started to show a progressive slow deactivation down to the activity observed in cycle 1, around 10 min^{-1} still in the full release of 3 equiv of H_2 (Figure 3).

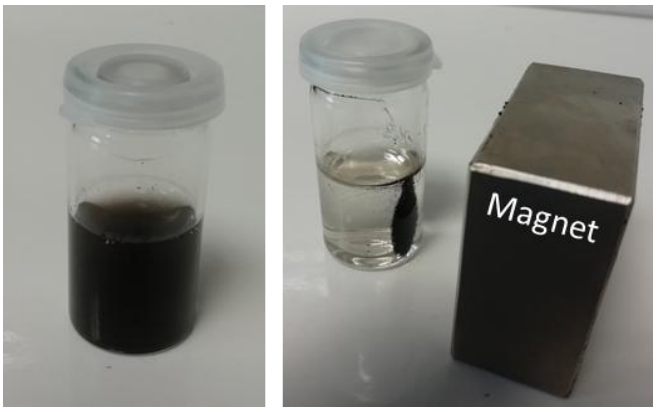

Figure 2. Recovering of 7%-Ru@Fe_3O_4 nanocomposite colloidal suspension (left) on application of a magnet block (right).

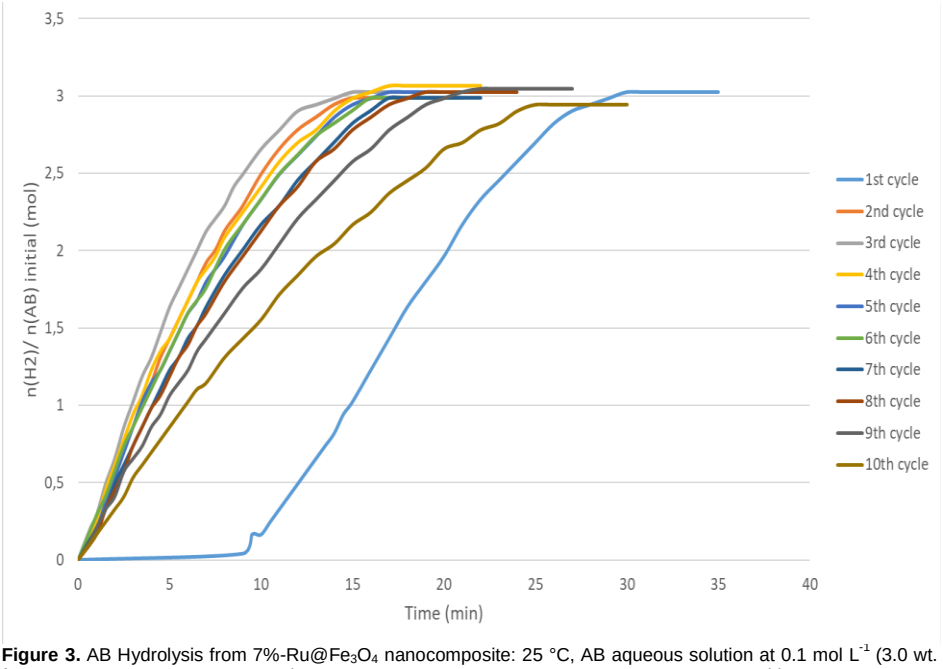

Cycle	TOF $(mol(H_2).mol(Ru)^{-1}.min^{-1})$
1	9.4
2	18.5
3	18.7
4	17.6
5	16.5
6	17.3
7	16.3
8	14.8
9	13.4
10	10.9

Figure 3. AB Hydrolysis from 7%-Ru@Fe_3O_4 nanocomposite: 25 °C, AB aqueous solution at 0.1 mol L^{-1} (3.0 wt. % of Ru/AB) over ten successive cycles reused from magnetic recovery without catalyst treatment.

Figure 4 shows a STEM HAADF image of 7%-Ru@Fe_3O_4 nanocomposites after 3 cycles of AB hydrolysis (at maximum activity). Such image allows for chemical analysis at atomic resolution, the contrast depending on the atomic number of the element, ruthenium is clearly distinguished in the picture by appearing brighter than iron. This result is confirmed by the chemical analysis along a line (red line in Figure 4 bottom) associated to the composition of the nanocomposite in Fe, O, and Ru. A perfect match is observed between the chemical composition and the position of the brightest nanoparticles visible in the image, allowing us to associate them definitively with Ru nanoparticles supported on iron oxide. The structural analysis based on the high-resolution image (Figure 4, top) clearly reveal different sets of lattice planes inside the Ru nanoparticles. The distance measured from Fourier transformation of the HRTEM image are *d* = 0.21, 0.14, 0.12, and 0.11 nm, within the accuracy of the measurements. These distances are in very good agreement with the (002), (110), (103), and (112) interplanar distances anticipated for Ru(0) hcp.

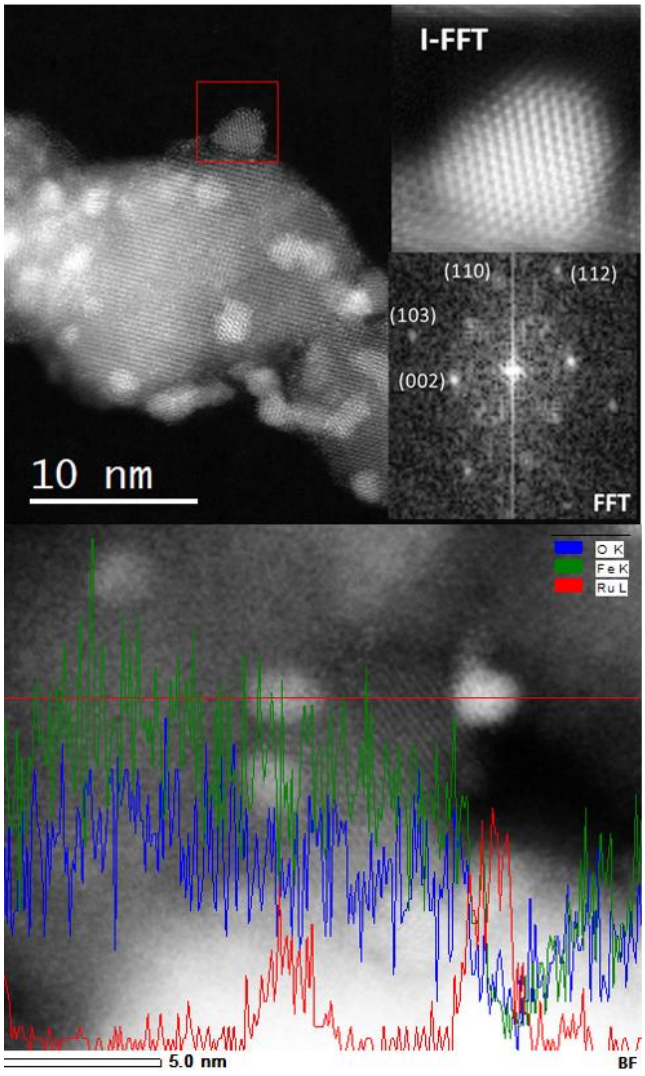

Figure 4: STEM HAADF images of 7%-Ru@Fe_3O_4 after AB hydrolysis highlighting the presence of hcp Ru NPs on the iron oxide support.

The induction time we observed in the first cycling run is associated to the initial presence of oxidized Ru species (oxides, hydroxides, or oxi-hydroxides) on the nanocomposite surface, as indicated by XPS. Thus, an activation of the surface species that is conserved along recycling, possibly results from the action at RT of ammonia-borane as a ruthenium reductant in water. XPS analysis of 7%-Ru@Fe_3O_4 nanocomposites after three cycles of AB hydrolysis in the BE area of C 1*s* and Ru 3d evidenced a clear shift to lower binding energy (*ca* 0.5 eV, see Figure S12), as well as a noticeable decrease of the full width at half maximum (FWHM). These changes clearly support ruthenium reduction due to AB action, and are consistent with STEM HAADF analysis. We also achieved a pretreatment of the 7%-Ru@Fe_3O_4 nanocomposite by $NaBH_4$ (1 h stirring in aqueous solution of 2 mol equiv. of $NaBH_4$ relative to Ru), which only slightly reduced this induction time for the first cycle (6 min, TOF 10.5 min^{-1}) but that sensibly improved the TOF up to 23.1 min^{-1} over the three following cycles.

Because the hydrolysis products from AB, like NH_4^+ or BO_2^- can accumulate on the surface of the Ru@SPIO and reduce the nanocatalyst performance,[36] we tentatively achieved a ten cycles experiment using a washing procedure of the catalyst surface at each run (Figure S13). For these experiments including the simple water rinsing of the catalyst, no special benefit was obtained with results consistent with the previous standard recycling, and demonstrating a similar profile over ten recycling in AB hydrolysis.

We tested the limitation of the nanocatalyst in terms of metal content by reducing the catalyst (Ru) /AB ratio to 0.3 wt. % instead of 3.0 wt. %, the other reaction parameters remaining unchanged (Figure S14). Two consecutive cycles were carried out. In this case, the catalyst activation time was increased to *ca* 20 min for the first cycle. The TOF of this first cycle was 21.0 min^{-1}, while that of the second cycle drop to 10.2 min^{-1}. Thus, at this low metal content, the activity of the catalyst was found to be high after the induction period, but the loss of efficiency occurs readily from the second cycle. Notably, the bubbler water pH was also checked for NH_3 ammonia release, and we did not observe any detectable change in the pH, confirming full H_2 release.[37]

We further investigated the performances of the Ru@SPIO catalytic system under various conditions of temperature (Figure S15) and AB concentration (Figure S16). Three successive AB hydrolysis catalytic cycles were achieved using our standard conditions (7%-Ru@Fe_3O_4, AB at 0.1 mol L^{-1}, 3.0 wt. % of Ru/AB) at temperatures ranging between 30 and 50 °C, every 5 °C. Their TOFs were estimated at each cycle. Unsurprisingly, the raise of reaction temperature was favorable to much faster H_2 evolution, thus: at 30 °C (TOF_{max} = 33.9 min^{-1}), 35 °C (TOF_{max} = 44.6 min^{-1}), 40 °C (TOF_{max} = 64.4 min^{-1}), 45 °C (TOF_{max} = 75.5 min^{-1}), and 50 °C (TOF_{max} = 86.3 min^{-1}) the rates consistently increased. The corresponding apparent activation energy was found at 36.0 kJ mol^{-1} (Figure S15), which ranges in the commonly found values for this reaction (values reported ranges from 12.0 to 80.0 kJ mol^{-1}).[13]

At 25 °C, the concentration of AB was varied at 0.02 M (five fold lower than 0.1 M) and 0.5 M (five fold higher than 0.1 M) under otherwise the same conditions (7%-Ru@Fe_3O_4, 3.0 wt. % of Ru/AB, Figure S16). The lower concentration 0.02 M [AB] was found unsuitable with an incomplete reaction; however, this might be also correlated with the lower (possibly limit) amount of Ru catalyst introduced. The higher concentration 0.5 M [AB] had mainly an effect on reducing the induction time (by a factor 4), while an otherwise TOF consistent with 0.1 M [AB] conditions was found (*ca* TOF 26 min^{-1}).

Hydrolysis of ammonia-borane under similar conditions (25 °C, aqueous solution of AB at 0.1 mol L^{-1} and 3.0 wt. % of catalyst (Ni)/AB using the Ni-based nanocomposite 7%-Ni@Fe_3O_4 (Figure S17) confirmed the reported lower intrinsic activity of nickel for AB hydrolysis.[13] Three consecutive catalytic cycles were performed, the first one started after several hours of induction (> 3 h). This time was reduced to *ca* 5 min in the 2nd cycle and 3 min in the 3rd cycle, consistent with TOFs ranging from 0.5 to 1.5 min^{-1}, and an evolution of 2.5 equiv of H_2 in 130 min in cycle 2, and 60 min in cycle 3.

Ammonia-borane methanolysis from metal nanocomposites based on magnetic iron oxide. H_2 release from AB in non-aqueous solvent is expected to facilitate the regeneration of starting material from by-products treatment ($NH_4B[OCH_3]_4$ formed from AB methanolysis is back converted to AB by reaction with metal hydrides at room temperature).[38] Thus, H_2 releasing from AB solvolysis in protic solvents such as methanol is worth developing. Notably, AB has superior solubility in methanol,[39] and methanolysis provides H_2 as single gaseous product without ammonia contamination. In addition, catalytic methanolysis of AB could be achieved at temperatures below 0 °C due to the low melting point of MeOH (facilitating H_2 supply in cold climate). Finally, AB in methanol has a high stability against uncontrolled self-releasing H_2 gas. Accordingly, methanolysis has been achieved successfully with nanocatalysts based on expensive Rh, Pt and Pd materials,[13] and more recently with other systems.[40] Methanolysis of AB has been also efficiently achieved with sophisticated nanocomposites based on small ruthenium NPs encapsulated in a crystalline porous coordination cage.[41,42] However, the large scale manufacturing of such MOF-based systems is rather doubtful because of their cost and preparation procedure, and the access to simpler low-cost systems is desirable. Thus, we investigated the performance of our recyclable commercial system on the methanolysis reaction. While Ni-based systems show no activity, we achieved AB methanolysis from 7%-Ru@Fe_3O_4 nanocomposite (25 °C, AB methanol solution at 0.1 mol L^{-1} (3.0 wt. % of Ru/AB) other eight successive cycles from magnetic recovery without any catalyst treatment (Figure 5). Surprisingly, the global efficiency for H_2 release was clearly superior to hydrolysis in terms of TOFs after the first cycle. Initially, without any pre-treatment of the nanocatalyst, a very long induction time around 80 min was necessary before significant H_2 evolution, while the full H_2 release was achieved in 150 min (TOF = 1.5 min^{-1}). However, after this first catalytic run, the nanocomposite was magnetically recovered and the supernatant syringed out. Without any further treatment, the subsequent run (2nd cycling) was achieved with a 0.1 mol L^{-1} fresh AB methanolic solution. We observed the disappearance of the induction time observed in the cycle 1, with an immediate H_2 evolution yielding three

equiv of H_2 in about 11 min, corresponding to an average TOF *ca* 27 min^{-1}. This performance was even majored in the 3rd cycle (TOF 31 min^{-1}) and conserved until the 7th cycle (17.9 min^{-1}) after which a significant performance drop is observed. To the best of our knowledge, for the few systems reporting on both hydrolysis and methanolysis, the latter was assumed a much more challenging reaction. Therefore, the results on methanolysis for the 7%-Ru@Fe_3O_4 nanocomposite matches the performances of current systems with inexpensive metals,[40] with in addition an excellent recyclability. Nevertheless, the deactivation process compared to hydrolysis occurs earlier in the cycles of reusing, suggesting that the side products and waste formed are more poisonous to the catalysts. The pre-treatment of the 7%-Ru@Fe_3O_4 nanocatalyst with $NaBH_4$ reduced the induction time of the first cycle to *ca* 50 min, while a catalyst washing workup after each recycling did not improve the TOF and recyclability of the system (Figure S18).

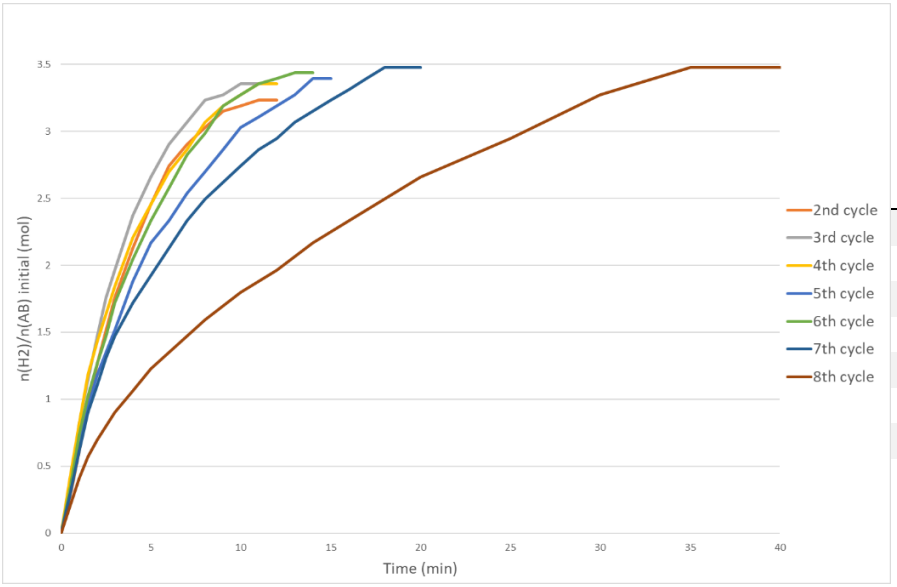

Cycle	*TOF* $(mol(H_2).mol(Ru)^{-1}.min^{-1})$
1	**1.5**
2	**27.2**
3	**31.1**
4	**28.3**
5	**22.5**
6	**24.5**
7	**17.9**
8	**9.2**

Figure 5. AB Methanolysis from 7%-Ru@Fe_3O_4 nanocomposite (25 °C, AB methanol solution at 0.1 mol L^{-1}, 3.0 wt. % of Ru/AB) other 8 successive cycles reused from magnetic recovery without catalyst treatmen

The full elucidation of the catalysis deactivation process from repeated cycling requires further advanced study; however, we examined the leaching by ICP-AES measurement of ruthenium and iron, as well as the production of waste in catalysis by ^{11}boron NMR. Over three runs, the ICP analyses of the filtrate after each hydrolysis run (see Table S3) have shown a decreasing degree of leaching of *ca* a one percent mass from initial amount: 1.3% (run 1), 0.7% (run 2) and 0.5% (run 3). Notably, the leaching of iron is proportionally superior since in the filtrate, after run 1, the concentration of iron is *ca* 12 times higher than the concentration of ruthenium (18.08 mg L^{-1} in Fe *vs* 1.48 mg L^{-1} in Ru). In run 2, this ratio Fe/Ru in the filtrate is of *ca* 16, and 20 for run 3. The limited degree of leaching in ruthenium does not induce strong variation in the TOFs in the first three cycles, and might not be ultimately responsible for catalysts main deactivation process.

The ^{11}B NMR analysis confirms that full conversion of AB occurred (AB is characterized by a chemical shift in D_2O of –23.8 ppm, $^1J_{BH}$ = 91 Hz, Figure S19), while the concomitant formation of polyborates mixture is identified from broad signals located at 8.3 and 11.9 ppm.[43,44,45] The broadness and shift of the signals slightly differs from the results recently reported by Tuba *et al*. for [$B_2O_7^{2-}$],[45] and are in better agreement with some equilibrium involving $B(OH)_3/B(OH)_4^-$ (8.3 ppm), and the triborate $B_3O_3(OH)_4^-$ with higher rank borates such as $B_4O_5(OH)_4^{2-}$ or $B_5O_6(OH)_4^-$ (11.9 ppm).[43,44]

Notably, descriptors of the catalysts performance that are complementary to TOF, and which can be extrapolated from Figure 3 (AB hydrolysis) and Figure 5 (AB methanolysis), are reported in Table S4 and Table S5, respectively. The turnover number (TON, mol_{H2}/mol_{Ru}) for each cycle allows to determine a cumulative total turnover number (TTO), estimated at TTO = 2790 after ten cycles for AB hydrolysis, and TTO = 2431 after eight cycles for AB methanolysis from 7%-Ru@Fe_3O_4. These TON values are obviously minored since they are calculated on the total Ru metal present and not corrected from true surface active species. The catalyst performance indicator [CPI = TON / {reaction time (h) x [Ru] (mM) x $[AB]_0$ (mM) }] recently proposed,[45] takes into account for a given catalyst, high TON, short reaction time and low concentration of catalyst and substrate. We found, over ten cycles, an average value of CPI = 8.5 and 11.3 for respectively AB hydrolysis and methanolysis over eight cycles, validating the superior activity for methanolysis.

Conclusion

Easily recoverable heterogeneous catalysts are promising for developing modern, environmentally-friendly, industrial processes in an appropriate “Hydrogen Energy Economy”. We

reported herein a Ru-based magnetically recyclable nanocomposite, 7%-Ru@Fe_3O_4, quickly recoverable by using a simple magnet block settling, which achieved for full H_2 release (3 molar equiv.) from AB hydrolysis, 10 catalytic cycles and for AB methanolysis 8 efficient catalytic cycling. Because of the large current industrial activity based on methanol, and the absolute need for high purification of waste water, methanol-based AB solvolysis is an attractive approach to be further developed for H_2 storing/release. Low-cost efficient catalysts such as describe herein participate to this effort.

Supplementary information available: survey of ruthenium-catalysts used for AB solvolysis; SEM, cartography and EDX of nanocomposites; TEM of SPIO support and nanocomposites; XPS of nanocomposites; Complementary time course of H_2 evolution from AB solvolysis catalytic reactions; Conditions for XPS analysis and TEM and STEM-HAADF analysis; Complementary structural data for nanocomposites (XRD, TEM-EDX, HR-TEM, elements mapping); ICP analysis; ^{11}B NMR of post-catalytic reaction mixture.

Experimental Section

All organic reagents and solvent were purchased from commercial suppliers and used without purifications. The identity and purity of the products were checked at the "Chemical Analysis platform" (PACSMUB) from the University of Burgundy. Metal Catalysts on SPIO were acquired from SON company (see for Ru@SPIO: https://www.sonsas.com/spio-ru-c2x36775005).

Catalytic hydrolysis of AB and nanocatalyst recycling. The hydrolysis reactions of AB were conducted in demineralized water at 25 °C, using a regulated bath. In a 20 mL Schlenk tube, the nanocatalyst (16 mg, metal/AB ratio 3.0 wt. %) was suspended in 8 mL of water with continuous stirring (1000 rpm). Then, 2 mL of an aqueous solution of AB 85% (35.5 mg, 1 mmol, 0.1 mol L^{-1}) was injected in the Schlenk tube, and timing started. The Schlenk tube is equipped with a gas outlet to a water-filled gas burette. The volume of dihydrogen released was monitored by measuring the displacement of water in the burette. A quantitative conversion of AB produced 3.0 equiv of H_2 at atmospheric pressure without ammonia contamination detected. The metal@SPIO was then recovered by magnetic settling, eventually washed three times with 2 mL of degassed and deionized water, and then could be immediately reused in a next cycle using a fresh AB solution.

Nanocatalyst reducing pretreatment with $NaBH_4$. The nanocomposite is stirred for 1 hour in an aqueous solution of $NaBH_4$ with a concentration of two molar equivalent relative to the metal attached to the SPIO. The metal@SPIO is then recovered by magnetic settling, and then washed 3 times with 2 mL of degassed and deionized water and then primary vacuum dried during 3 hours.

Catalytic methanolysis of AB and nanocatalyst recycling. The methanolysis reactions were conducted using the same set-up and temperature controlled conditions as hydrolysis by replacing water by methanol (metal/AB ratio fixed 3.0 wt. %, [AB] = 0.1 mol L^{-1} in MeOH analytical grade).

Acknowledgements:
This work was supported by the CNRS (LCC, ICMUB and ICB), the Université de Bourgogne, the Conseil Régional Bourgogne Franche-Comté, and the PIA-excellence ISITE-BFC (COMICS project "Chemistry of Molecular Interactions Catalysis and Sensors" (FEDER). The Fonds Européen de Développement Régional and the graduate school EUR-EIPHI supported this program through *ProdHyg* project "Secured Hydrogen Production". Thanks is due to PACSMUB platform for the analytical work including ICP and ^{11}B NMR (M. Heydel, M.-J. Penouilh, Q. Bonnin).

Contributor Roles

J.-C.H., M.L.K., D.P., P.-E.D. and J.P. conceived this program. P.-E.D. and J.P. synthesized the magnetic (iron oxide)-based nanoparticles. A.B. and D.P. conceived and performed ammonia-borane solvolysis and catalytic recycling. M.L.K. and V.C. achieved and analyzed microscopy. M.B., B.D. and O.H. achieved and analyzed X-ray spectroscopy. Under J.-C.H. guidance, all authors contributed to the discussions, the manuscript writing and approved the final manuscript.

Conflict of Interest

The authors declare the following competing financial interest(s): P.-E. D. and J. P. are co-founder of the commercial company SON (https://synthesisofnanohybrids.com/en/) which develops and commercializes the present iron oxide-supported nanocatalysts.

Keywords: ammonia-borane • hydrogen • magnetic recycling • methanolysis • ruthenium nanocomposite

Table of Contents Graphic and Text

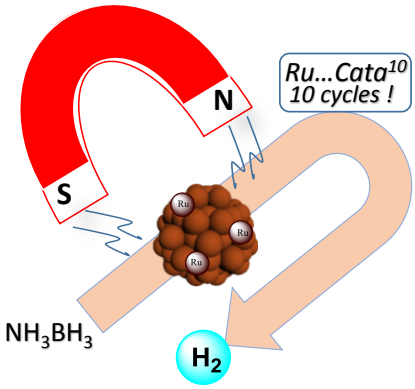

Ru@Fe_3O_4 nanocomposites displayed high recyclability over ten runs for the production at room temperature (25 °C) of three equiv dihydrogen H_2 from ammonia-borane H_3NBH_3, either from hydrolysis or methanolysis fast reactions. The nanocatalyst maintains consistent turnover frequencies while is operated very simple magnetic recovering without any further treatment.

Automated References

[1]. P. T. Anastas, M. M. Kirchhoff, T. C. Williamson, *Appl. Catal., A: Gen.* **2001**, *221*, 3–13.

[2]. P. T. Anastas, M. M. Kirchhoff, *Acc. Chem. Res.* **2002**, *35*, 686–694.

[3]. H. C. Erythropel, J. B. Zimmerman, T. M. de Winter, L. Petitjean, F. Melnikov, C. H. Lam, A. W. Lounsbury, K. E. Mellor, N. Z. Janković, Q. Tu, L. N. Pincus, M. M. Falinski, W. Shi, P. Coish, D. L. Plata, P. T. Anastas, *Green. Chem.* **2018**, *20*, 1929–1961.

[4]. C. Sanchez, P. Belleville, M. Popall, L. Nicole, *Chem. Soc. Rev.*, **2011**, *40*, 696–753.

[5]. R. K. Sharma, S. Dutta, S. Sharma, R. Zboril, R. S. Varma, M. B. Gawande, *Green Chem.*, **2016**, *18*, 3184–3209.

[6]. M. S. Mauter, M. Elimelech, *Environ. Sci. Technol.* **2008**, *42*, 5843–5859.

[7]. D. Astruc, F. Lu, J. R. Aranzaes, *Angew. Chem. Int. Ed.* **2005**, *44*, 7852–7872.

[8]. R. B. N. Baig, R. S. Varma, *Chem. Commun.*, **2013**, *49*, 752–770.

[9]. B. Karimi, F. Mansouri, H. M. Mirzaei, *ChemCatChem* **2015**, *7*, 1736–1789.

[10]. P. Vandezande, L. E. M. Gevers, I. F. J. Vankelecom, *Chem. Soc. Rev.* **2008**, *37*, 365–405.

[11]. D. Astruc, K. Heuzé, S. Gatard, D. Méry, S. Nlate, L. Plault, *Adv. Synth. Catal.* **2005**, *347*, 329–338.

[12]. D. Wang, D. Astruc, *Chem. Rev.* **2014**, *114*, 6949−6985.

[13]. C. D. Mboyi, D. Poinsot, J. Roger, K. Fajerwerg, M. L. Kahn, J.-C. Hierso, *Small* **2021**, 2102759.

[14]. J.-M. Yan, X.-B. Zhang, S. Han, H. Shioyama, Q. Xu, *Angew. Chem. Int. Ed.* **2008**, *47*, 2287–2289.

[15]. J. Manna, S. Akbayrak, S. Özkar, *Appl. Catal., B: Env.* **2017**, 208, 104–115.

[16]. H. Jia, X.-J. Liu, X. Chen, X.-X. Guan, X.-C. Zheng, P. Liu, *Int. J. Hydrogen Energy* **2017**, *42*, 28425–28433.

[17]. S. Akbayrak, G. Çakmak, T. Öztürk, S. Özkar, *Int. J. Hydrogen Energy* **2021**, 46, 13548–13560.

[18]. X. Cui, H. Li, G. Yu, M. Yuan, J. Yang, D. Xu, Y. Hou, Z. Dong, *Int. J. Hydrogen Energy* 2017, 42, 27055–27065.

[19]. Y. Tonbul, S. Akbayrak, S. Özkar, *J. Colloid Interface Sci.* **2019**, *553*, 581–587.

[20]. S. Akbayrak, Y. Tonbul, S. Özkar, *ACS Sustainable Chem. Eng.* **2020**, *8*, 4216–4224.

[21]. K. Aranishi, H.-L. Jiang, T. Akita, M. Haruta, Q. Xu, *Nano Res.* **2011**, *4*, 1233–1241.

[22]. Z.-H. Lu, J. Li, A. Zhu, Q. Yao, W. Huang, R. Zhou, R. Zhou, X. Chen, *Int. J. Hydrogen Energy* **2013**, *38*, 5330–5337.

[23]. W. Feng, L. Yang, N. Cao, C. Du, H. Dai, W. Luo, G. Cheng, *Int. J. Hydrogen Energy* **2014**, *39*, 3371–3380.

[24]. L. Yang, J. Su, W. Luo, G. Cheng, *ChemCatChem* **2014**, *6*, 1617–1625.

[25]. D. R. Abd El-Haiz, G. Eshaq, A. E. ElMetwally, *Mater. Chem. Phys.* **2018**, *217*, 562–569.

[26]. S. Cheng, Y. Liu, Y. Zhao, X. Zhao, Z. Lang, H. Tan, T. Qiu, Y. Wang, *Dalton Trans.* **2019**, *48*, 17499–17506.

[27]. R. Lu, C. Xu, Z. Yang, L. Zhou, J. Wu, Y. Wang, Y. Zhang, G. Fan, *Int. J. Hydrogen Energy* **2020**, *45*, 1640–1648.

[28]. J. Chen, Z.-H. Lu, Y. Wang, X. Chen, L. Zhang, *Int. J. Hydrogen Energy* **2015**, *40*, 4777–4785.

[29]. J. Zhan, Y. Duan, Y. Zhu, Y. Wang, H. Yao, G. Mi, *Mater. Chem. Phys*. **2017**, 201, 297–301.

[30]. S. Akbayrak, O. Taneroglu, S. Özkar, *New J. Chem.* **2017**, *41*, 6546–6552.

[31]. J. Manna, S. Akbayrak, S. Özkar, *J. Colloid Interface Sci.* **2017**, *508*, 359–368.

[32]. N. Shaikh, A. Helal, A. N. Kalanthoden, B.Najjar, Md. A. Aziz, H. D. Mohamedd, *Catal. Commun.* **2019**, *119*, 134–138.

[33]. D.J. Morgan, Surf. Interface Anal. 2015, 47, 1072–1079

[34]. A. M. Beccaria, G. Castello, G. Pogg, *Br. Corros. J*., **1995**, *30*, 283–287.

[35]. M.C.Biesinger, B.P. Payne, L.W.M. Lau, A. Gerson, R.St.C. Smart, Surf. Interface Anal. 2009,41, 324–332

[36]. We examined by TEM the catalyst changes (see the Supporting Information) after three cycling runs, which conserved a good dispersion of small nanoparticles suggesting that surface poisoning by N,B side-products or re-oxidation of surface Ru might be involved in the progressive deactivation process.

[37]. V. R. Bakuru, B. Velaga, N. R.Peela, S. B. Kalidindi, *Chem. Eur. J.* **2018**, *24*, 15978–15982.

[38]. P. Veeraraghavan, P. D. Gagare, *Inorg. Chem.* **2007**, *46*, 7810–7817.

[39]. M. P. Confer, A. DeSimone, H. Burnham, W. McLeod, T. M. Klein, S. C. Street, D. A. Dixon, *Int. J. Hydrogen Energy* **2021**, *46*, 10801–10808.

[40]. S. Özkar, *Int. J. Hydrogen Energy* **2020**, *45*, 788–7891.

[41]. Y. Fang, J. L. Li, T. Togo, F. Y. Jin, Z. F. Xiao, L. J. Liu, H. Drake, X. Z. Lian, H. C. Zhou, *Chem* **2018**, *4*, 555–563.

[42]. Y. Wang, J.-L. Li, W.-X. Shi, Z.-M. Zhang, S. Guo, R. Si, M. Liu, H.-C. Zhou, S. Yao, C.-H. An, T.-B. Lu, *Adv. Energy Mater*. **2020**, 2002138–11.

[43]. J. Hannauer, U. B. Demirci, C. Geantet, J. M. Herrmann, P. Miele, *Phys. Chem. Chem. Phys*., **2011**, *13*, 3809–3818

[44]. G. Moussa, R. Moury, U. B. Demirci, P. Miele, *Int. J. Hydrogen Energy* **2013**, *38*, 7888–7895.

[45]. M. Nagyházi, G. Turczel, P. T. Anastas, R. Tuba, *ACS Sustainable Chem. Eng.* **2020**, *8*, 16097−16103.